JOURNAL OF SOLID STATE CHEMISTRY **121,** 339–349 (1996)
ARTICLE NO. 0046

Synthesis and Characterization of New Oxide Hydrates $H_x(V_xMo_{1-x})O_3 \cdot 0.3H_2O$ and $H_{0.27}(V_{0.27}W_{0.73})O_3 \cdot 1/3H_2O$

Loïc Dupont, Dominique Larcher, François Portemer, and Michel Figlarz†

Laboratoire de Réactivité et de Chimie des Solides, URA CNRS 1211, Université de Picardie Jules Verne, 33 rue Saint-Leu, 80039 Amiens, France

Received October 2, 1995; accepted October 3, 1995

From acid solutions obtained by dissolution of molybdenum or tungsten metal and V_2O_5 in hydrogen peroxide solution, pure and well-crystallized phases have been prepared under the general formula $H_xV_xMo_{1-x}O_3 \cdot 0.3H_2O$ ($0.06 \leq x \leq 0.18$) and $H_{0.27}V_{0.27}W_{0.73}O_3 \cdot 1/3H_2O$. The former presents an hexagonal structure (for instance, when $x = 0.13$, $a = 10.6129(5)$ Å, $c = 3.7045(3)$ Å, and space group $P6_3$) and the latter is isostructural with orthorhombic $WO_3 \cdot 1/3H_2O$ ($a = 7.272(1)$ Å, $b = 12.573(2)$ Å, $c = 7.728(1)$ Å, and space group $Fmm2$). These phases have been characterized by classic solid state techniques and their thermal behavior has also been studied.

I. INTRODUCTION

Metastable forms of MoO_3 and WO_3 have been synthesized in our lab by dehydration of the precursors $MoO_3 \cdot 1/3H_2O$ (1) and $WO_3 \cdot 1/3H_2O$ (2), respectively. The dehydration of the former leads to MoO_3 which crystallizes in the monoclinic system and shows a distorted ReO_3 structural type (3). The WO_3 hexagonal form (h-WO_3) is obtained by dehydration of $WO_3 \cdot 1/3H_2O$ (2). Many attempts have been made to prepare isomorphs of the MoO_3 hexagonal form (h-MoO_3). h-WO_3 and h-$Mo_{1-x}W_xO_3$ (4) are of great interest because of the potential applications due to their open structure: catalyst, host framework, and electrochemical possibilities (5, 6).

Several papers have been published concerning the preparation and the characterization of hexagonal MoO_3 isomorphs (7, 8, 9). Prepared by solid state methods, these phases are most often stabilized by large cations located in the channels which are parallel to the *c* axis. To compensate for the positive charges due to the cations, it is sufficient to partially substitute molybdenum (VI) for vanadium (V) in the structure. Then, these phases present the general formula $A_x(V_xMo_{1-x})O_3$ with A = K, NH_4, Rb, or Cs and the x value varied from 0.11 to 0.14 (10, 11). However, by using such a synthesis method, it is not possible to completely deintercalate the A cations (9, 10, 12). More recently, Hu and Davies (13) successfully prepared a vanadium stabilized open form of h-MoO_3 by precipitation from aqueous solutions and leaching of the so-obtained phase. The complete dehydration of the protonic precursor $H_{0.13}(V_{0.13}Mo_{0.87})O_3 \cdot 0.26H_2O$ leads to the $(V_{0.13}Mo_{0.87})O_{2.935}$ phase with retention of the open h-MoO_3 structure.

Using a similar method of preparation, Gopalakrishnan *et al.* (14) synthesized two hydrated phases which show the formula $H_{0.125}(V_{0.125}W_{0.875})O_3 \cdot 1.5H_2O$, isostructural with $WO_3 \cdot 2H_2O$, and $H_{0.33}(V_{0.33}W_{0.67})O_3 \cdot 1/3H_2O$, related to $WO_3 \cdot 1/3H_2O$. By dehydration of the latter, they have obtained $H_{0.33}(V_{0.33}W_{0.67})O_3$ which retains the hexagonal WO_3 structure.

On the other hand, hexagonal tungsten bronzes have been synthesized from tungstic acid solutions prepared by dissolution of metallic tungsten in hydrogen peroxide solution (15). From these works, we have found a new and rather simple method of synthesis which allows for the preparation of many hydrated oxides within the V–Mo–O system and a new hydrated oxide within the V–W–O system.

In this paper, we present results related to the preparation and the characterization of the hydrated phases $H_xV_xMo_{1-x}O_3 \cdot 0.3H_2O$ (with $0.06 \leq x \leq 0.18$) and $H_{0.27}V_{0.27}W_{0.73}O_3 \cdot 1/3H_2O$. These phases are obtained pure by dissolution of metallic molybdenum or tungsten (M) and vanadium pentaoxide in hydrogen peroxide solution. We study the influence of the total metallic concentration [V + M] in solution and that of the [V]/[M] ratio on the number and the nature of the precipitated phases and their chemical composition. Dehydration products are also described.

II. METHODS OF SYNTHESIS

It is well known that alkali compounds may play an important role in the stabilization of such structures. Therefore, it was important to prevent any cause of contamination by Na in our reactions. It was noted that the cumulative alkali content in all the reagents (water, H_2O_2, Mo, W, V_2O_5, and HNO_3) indicates only traces of Na, Li, K, and Ca. In order to prevent further contamination by

† Deceased.

0022-4596/96 $18.00

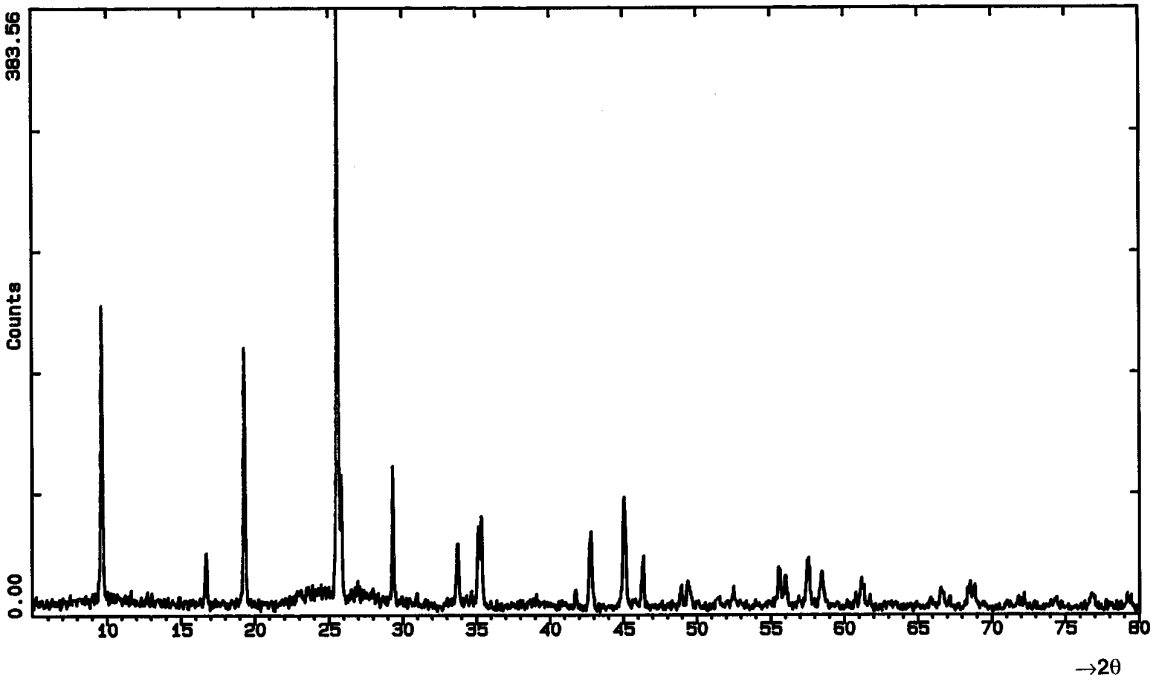

FIG. 1. X-ray diffraction pattern of phases in the V–Mo–O system obtained without addition of strong acid.

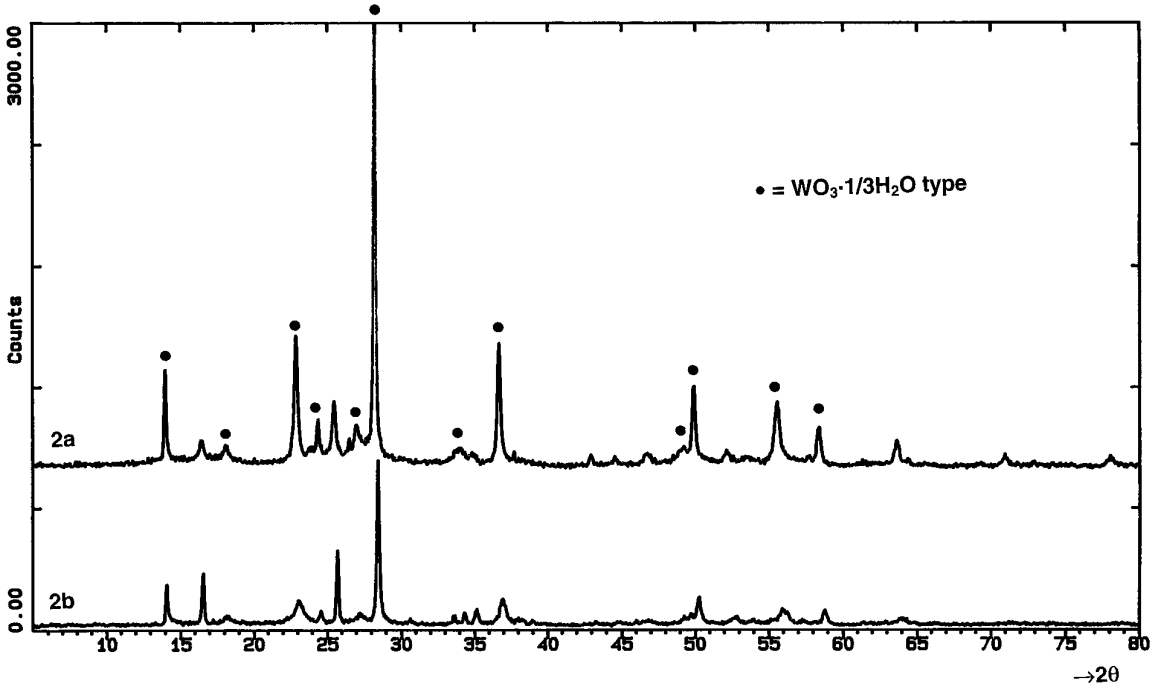

FIG. 2. X-ray diffraction pattern of phases in the V–W–O system obtained (a) without addition of strong acid and (b) with [V + W] = 0.12 *M*.

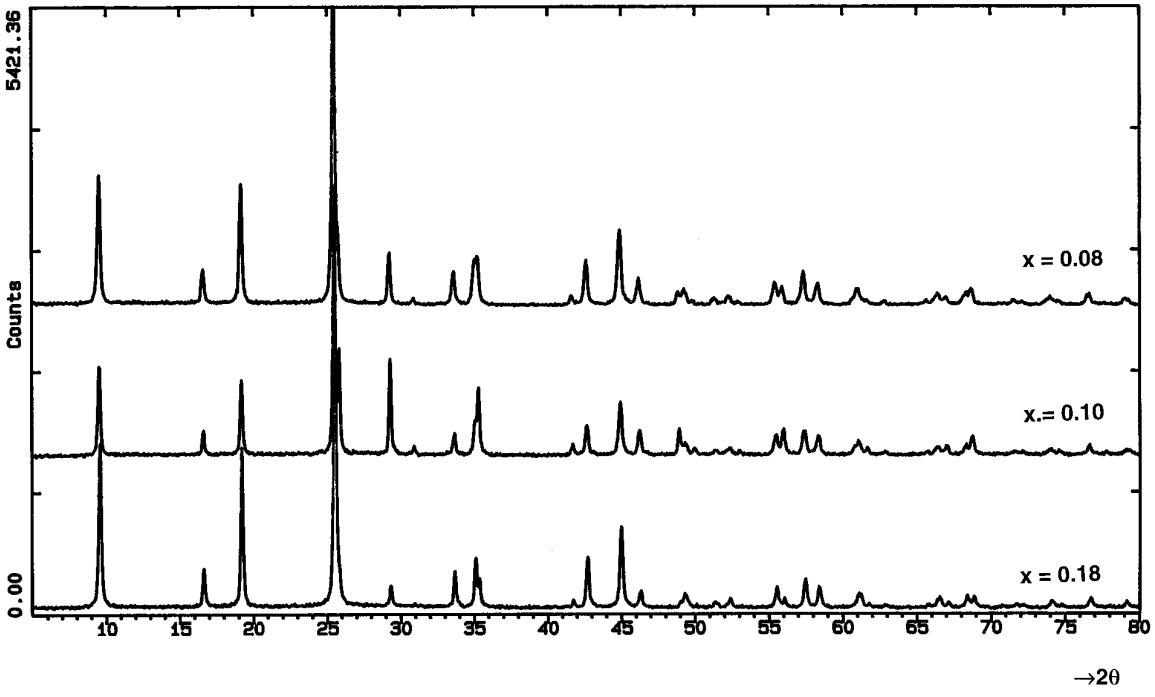

FIG. 3. X-ray diffraction patterns from $H_xV_xMo_{1-x}O_3 \cdot 0.3H_2O$ for three x values: 0.08, 0.10, and 0.18.

Na, all the following experiments were performed in inox vessels. The studies of our resulting powders for alkali contents by atomic absorption have indicated a very small amount of Na (V/Na $>$ 50) in all our powders.

(*a*) *Dissolution of Reagents*

Tungsten (PROLABO 99.9%) or molybdenum (PROLABO 99.9%) was first dissolved in 250 ml of an aqueous solution of 10% hydrogen peroxide (MERCK) with a pH value close to 1.5. During the exothermic dissolution, the H_2O_2 solution changed from colorless to a translucent yellow-orange color. After the solution cooled to room temperature, V_2O_5 (Aldrich-Chemie) was added to the molybdic (or tungstic acid) solution which became orange in both cases. After complete dissolution of the different solid phases, the pH value of the solution was close to 1. Then, the solution was acidified by addition of few milliliters of a strong mineral acid (HNO_3) up to a pH value of about 0.7 and heated under magnetic stirring at 50°C in order to eliminate excess hydrogen peroxide. In the case of a simultaneous dissolution of Mo (or W) and V_2O_5, the dissolution of the V_2O_5 is very irregular. This unreproductibility can be ascribed to the conjugated effects of the thermal exothermic effect and the acidification of the solution. The successive dissolution of both compounds Mo (or W) and V_2O_5 with intermediate cooling can avoid this phenomenon.

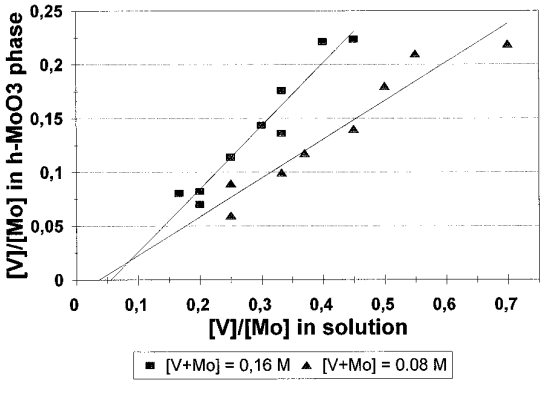

FIG. 4. $(V/Mo)_{solid}$ versus $[V]/[Mo]_{solution}$.

(*b*) *Precipitation*

(α) *V–Mo–O system.* The solution was heated under magnetic stirring at the boiling point to partially evaporate the solvent. The solution quickly became cloudy and heating was stopped when 100 ml of the solution remained in the inox vessel. After the solution cooled, the precipitate was washed with water, filtered on paper (WHATMAN no. 1), and dried at 50°C. The solid phase was pale yellow.

(β) *V–W–O system.* The solution was heated under magnetic stirring and refluxing at 70°C. Although a precipitate appeared after 2 hr, the reaction was stopped after 1

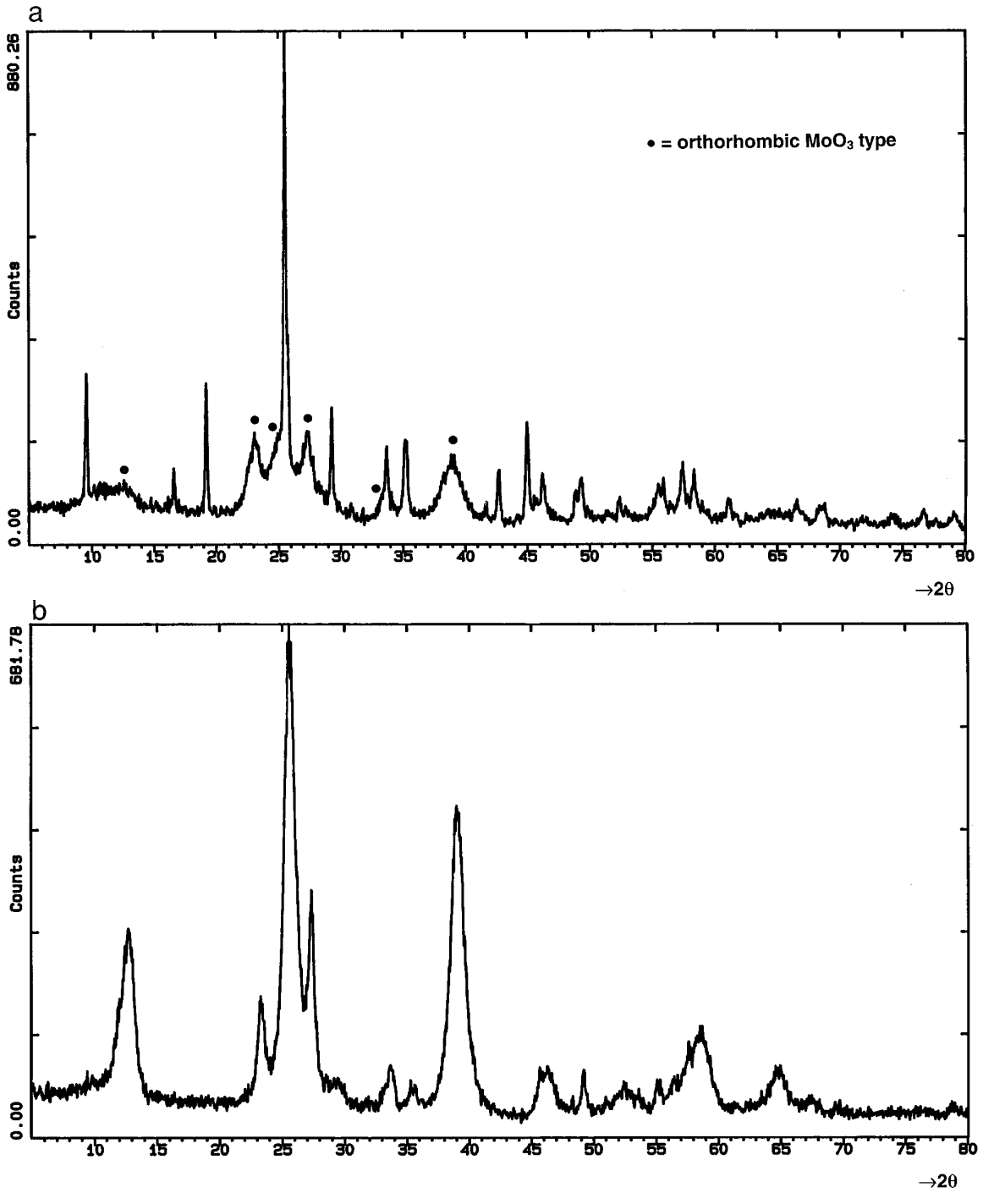

FIG. 5. X-ray diffraction pattern of phases in the V–Mo–O system obtained (a) with [V]/[Mo] = 1/7, (b) in the molybdenum rich part, and (c) with [V]/[Mo] over 1/2.

week for reasons exposed in the microscopy section. After the solution cooled, the precipitate was washed with bipermuted water, filtered through a MILLIPORE 0.2-mm filter, and dried at 50°C. In this case, the solid phase was yellow-green.

III. EXPERIMENTAL TECHNIQUES

Phase identification was carried out by X-ray diffraction (XRD) techniques using the powder method with an Inel CPS 120 diffractometer (Cu$K\alpha_1$) and the parameters re-

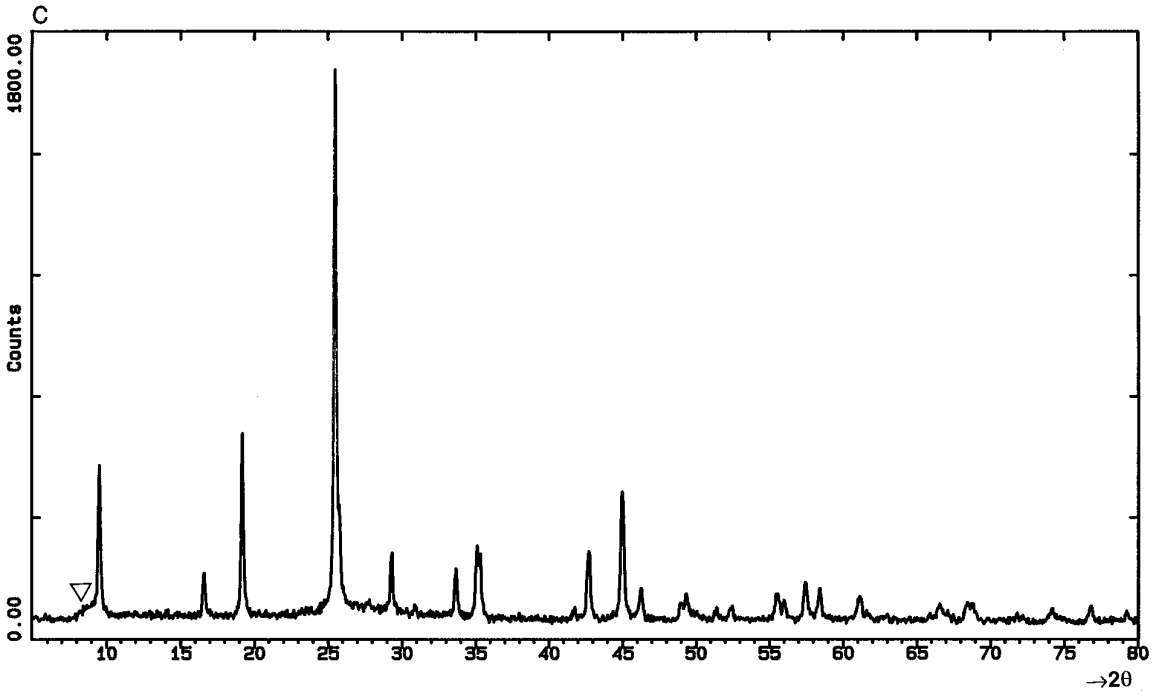

FIG. 5—*Continued*

finement was performed with data from a D5000 Siemens diffractometer using Bragg–Brentano geometry, with monochromatic Cu$K\alpha_1$ (λ = 1.540598 Å). The collected data were processed by means of a PC software package DIFFRAC-AT supplied by Siemens/Socabim. For all phases, relative metal composition was obtained from atomic absorption results, using a 3030 Perkin–Elmer spectrophotometer, in connection with thermal analysis results collected on a Setaram TG-DTA 92 and a Mettler TC11 apparatus for thermogravimetry (TG). Elemental compositions were rounded off by the Centre of Analysis of CNRS (BP 22-69390 VERNAISON). Electron micrographs were taken on a Philips SEM 505 scanning electron microscope (SEM) and on a JEOL 200 CX transmission electron microscope (TEM) equipped with a double-tilt goniometer stage (±10°). Samples were prepared from an acetone or 1-butanol suspension, dispersed by ultrasonic treatment, and then deposited onto copper grids coated with holely carbon films. Residual astigmatism is corrected by observation of the optical FFT of the amorphous carbon film.

IV. RESULTS AND DISCUSSION

Parameters like the pH of the solution, the [V]/[*M*] ratio, and the total metal concentration [V + *M*] play a very important role on the formation of the precipitates and on their chemical composition. These points are now developed in the following sections.

(*a*) *Influence of the pH of the Solution*

If the pH of the solution (after the dissolution of reagents in hydrogen peroxide) is greater than the value of 1, a coprecipitation occurs: an amorphous phase and an hexagonal MoO_3-type phase are observed in the case of V–Mo solutions (Fig. 1) while a precipitation of a phase mixture

TABLE 1
Nature of the Precipitate versus X = [V]/[Mo]

$X = 0$	$X = 1/20$	$1/6 < X < 1/20$	$1/6 \leq X < 1/2$	$1/2 \leq X$
$H_2MoO_5 \cdot H_2O$	α-MoO_3 type	α-MoO_3 type + h-MoO_3 type	h-MoO_3 type	h-MoO_3 type + amorphous phase

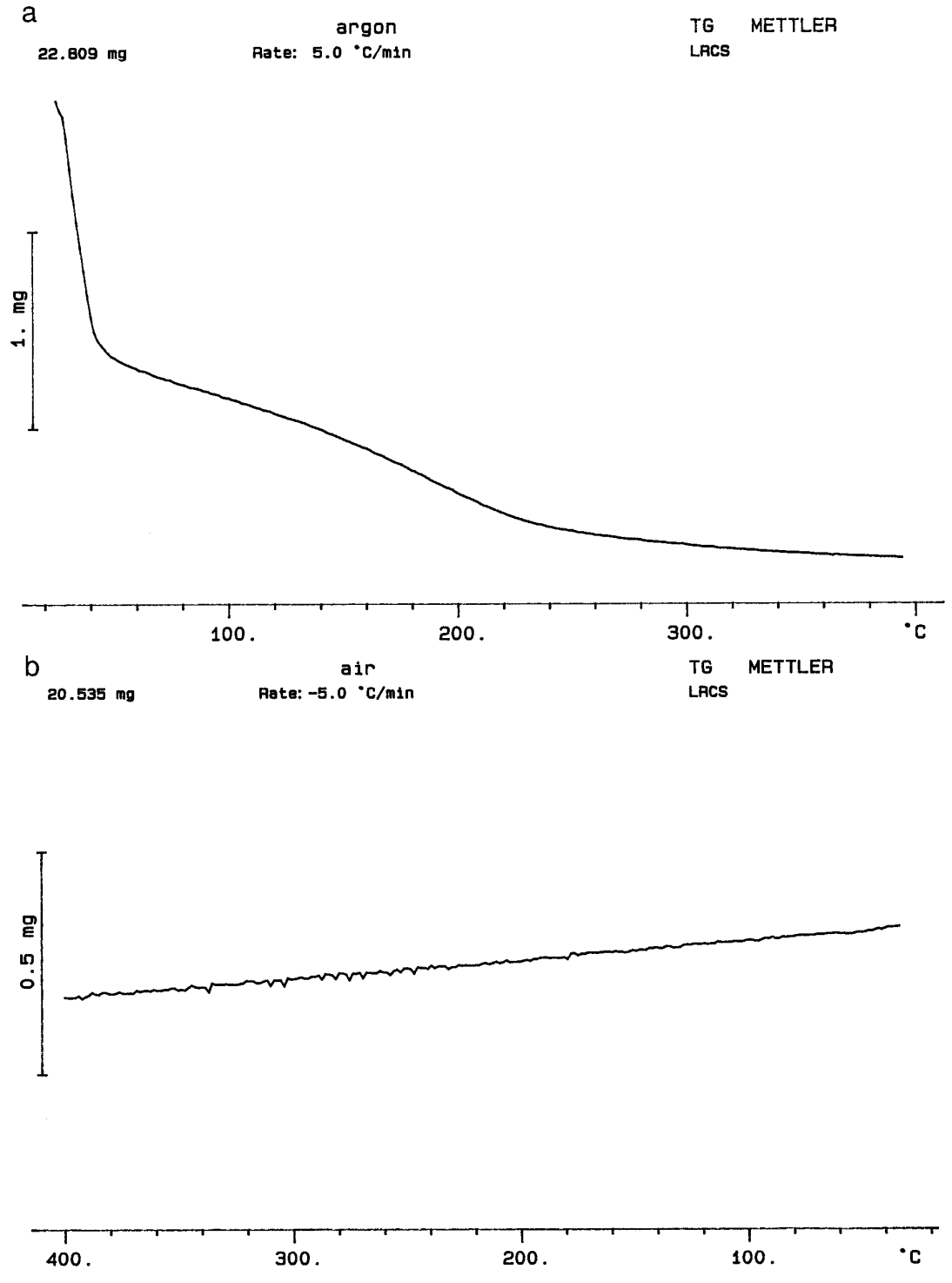

FIG. 6. (a) TGA curve of $H_{0.13}V_{0.13}Mo_{0.87}O_3 \cdot nH_2O$ phase. (b) cooling treatment performed from 450°C to room temperature.

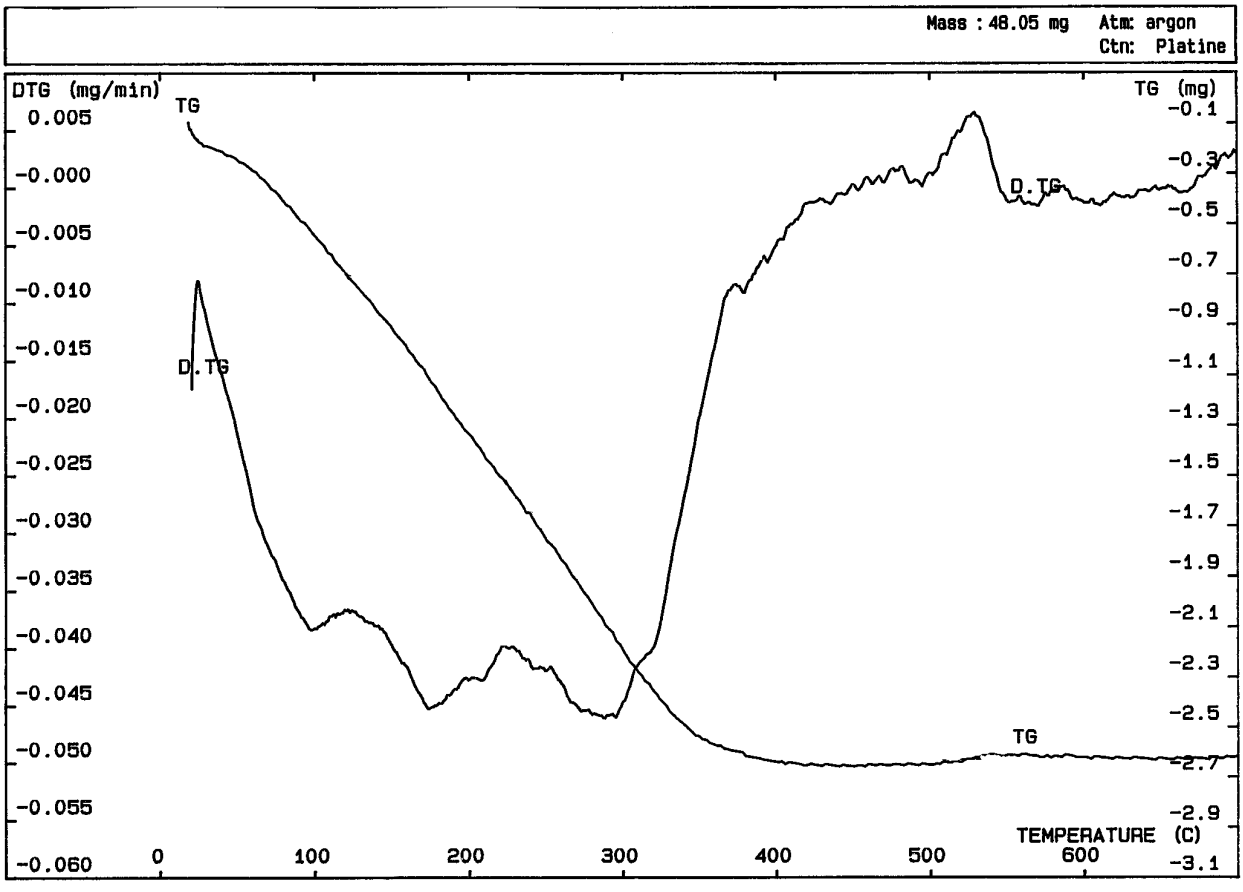

FIG. 7. TGA curve of the $H_{0.27}V_{0.27}W_{0.73}O_3 \cdot 1/3H_2O$ phase.

TABLE 2
XRD Data of $H_{0.13}V_{0.13}Mo_{0.87}O_3 \cdot 0.3H_2O$

h	k	l	$d_{obs.}$ (Å)	$2\theta_{obs.}$ (°)	$2\theta_{calc.}$ (°)	$\Delta(2\theta)$	$I_{obs.}$
1	0	0	9.20	9.604	9.615	0.011	12.8
1	1	0	5.307	16.690	16.693	0.003	11.2
2	0	0	4.598	19.290	19.299	0.009	32.1
2	1	0	3.474	25.618	25.622	0.004	100
1	0	1	3.436	25.909	25.910	0.001	33.5
1	1	1	3.038	29.375	29.380	0.005	42.4
2	0	1	2.884	30.981	30.981	0.000	3.9
2	2	0	2.6526	33.763	33.754	−0.009	10.2
3	1	0	2.5492	35.176	35.177	0.001	11.4
2	1	1	2.5339	35.395	35.394	−0.001	26.7
2	2	1	2.1574	41.839	41.845	0.006	4.4
3	2	0	2.1087	42.851	42.854	0.003	15.2
4	1	0	2.0058	45.168	45.171	0.003	26.4
4	0	1	1.9527	46.467	46.468	0.001	15.2
0	0	2	1.8522	49.149	49.148	−0.001	12.1
5	0	0	1.8380	49.554	49.548	−0.006	4.9
3	2	1	1.8322	49.722	49.713	−0.009	1.7
1	0	2	1.8157	50.205	50.204	−0.001	2.5

identified as isotypes of $WO_3 \cdot 1/3H_2O$ and $WO_3 \cdot 1H_2O$ was obtained in the case of V–W solutions (Fig. 2).

(*b*) *Effect of the Concentration of* [*V + Mo*] *as well as the* [*V*]/[*Mo*] *Ratio*

(α) *V–Mo–O system.* The combination of the [V + Mo] and [V]/[Mo] parameters makes it possible to have the widest domain of stability for the h-MoO_3-type phases. For a total metal concentration [V + Mo] = 0.16 *M*, the h-MoO_3 phases are quite stable when the [V]/[Mo] ratio in solution ranges from 0.16 to 0.45. To prepare a pure hexagonal phase with a [V]/[Mo] ratio over 0.45, the total metallic concentration must be reduced. After optimization of these two parameters, the stability domain of h-MoO_3 phases is extended now for [V]/[Mo] from 0.16 to 0.70 (Fig. 3) when [V + Mo] remains within the range from 0.08 to 0.16 *M*.

Atomic absorption can be indirectly used to show the existence of a solid solution. The (V/Mo) ratio in the solid phases is dependent on one hand on the total metallic concentration in solution and on the other hand on the [V]/[Mo] ratio in solution. In the 0.16–0.70 range, the phases

TABLE 3
XRD Data of $H_{0.27}V_{0.27}W_{0.73}O_3 \cdot 1/3H_2O$

h	k	l	$d_{obs.}$ (Å)	$2\theta_{obs.}$ (°)	$2\theta_{calc.}$ (°)	$\Delta(2\theta)$	$I_{obs.}$
0	2	0	6.289	14.072	14.074	0.002	17.1
1	1	1	4.885	18.147	18.158	0.011	18.8
0	0	2	3.863	23.006	23.003	−0.004	42.6
2	0	0	3.636	24.458	24.447	−0.011	6.5
0	2	2	3.292	27.061	27.068	0.007	<1
1	3	1	3.287	27.106	27.106	0.000	16.3
2	2	0	3.147	28.332	28.319	−0.014	100
2	0	2	2.6476	33.829	33.816	−0.013	6.2
2	2	2	2.4416	36.780	36.793	0.013	41.2
1	1	3	2.3836	37.708	37.705	−0.004	<1
2	4	0	2.3776	37.808	37.790	−0.018	4.1
3	1	1	2.2761	39.561	39.566	0.005	7.7
1	5	1	2.2711	39.653	39.638	−0.014	<1
1	3	3	2.1016	43.002	43.018	0.016	<1
0	6	0	2.0957	43.130	43.128	−0.002	3.6
3	3	1	2.0277	44.653	44.696	0.042	4.5
0	0	4	1.9321	46.992	47.004	0.013	4.4
0	2	4	1.8465	49.313	49.313	0.001	<1
0	6	2	1.8399	49.501	49.435	−0.066	2.5
4	0	0	1.8179	50.140	50.106	−0.034	24.8
2	6	0	1.8166	50.178	50.196	0.018	
1	5	3	1.7459	52.360	52.334	−0.026	3.3
2	0	4	1.7055	53.699	53.681	−0.019	4.5
3	5	1	1.7037	53.760	53.788	0.028	

present the general chemical formula $H_xV_xMo_{1-x}O_3 \cdot nH_2O$ with $0.06 \leq x \leq 0.18$. For a given total concentration, the relation between $(V/Mo)_{solid}$ and $[V]/[Mo]_{solution}$ is almost linear. Moreover, the straight lines obtained for two different total metallic concentrations are convergent (Fig. 4). The intersection point is close to the x axis, therefore it should be possible to synthesize a pure h-MoO_3 form. Nevertheless, in the case of a pure molybdenum solution, the product of the precipitation that is the hydrogen molybdenum peroxide hydrate $H_2MoO_5 \cdot H_2O$ (PDF no. 41-0060) is different from the expected h-MoO_3 form. For all [V]/[Mo] ratios in the 1/20 to 1/6 range, the XRD patterns show that an additional phase identified as α-MoO_3-type precipitates with the hexagonal-type phase (Fig. 5a). In the molybdenum rich part, the reaction product is a pale yellow phase badly crystallized and isostructural to the thermodynamically α-MoO_3 stable form (Fig. 5b). Up to now, with a total concentration [V + Mo] = 0.16 *M*, if the ratio [V]/[Mo] is increased over 1/2, an amorphous phase precipitates simultaneously with that of the h-MoO_3 type (Fig. 5c). These results are summarized in Table 1.

(β) *V–W–O system.* For a total metal concentration [V + W] > 0.08 *M*, a precipitation of a phase mixture is always observed. These phases are identified as isotypes of $WO_3 \cdot 1/3H_2O$ and $WO_3 \cdot 1H_2O$ (Fig. 2). In the case of a total metallic concentration [V + W] ≤ 0.08 *M*, a single orange phase isotype of $WO_3 \cdot 1/3H_2O$ is obtained whatever the $[V]/[W]_{solution}$. In this case, the product amount is highly dependent on the [V]/[W] ratio in contrast to the observed $H_x(V_xMo_{1-x})O_3 \cdot nH_2O$ product amount which is not dependent on the [V]/[Mo].

(*c*) *Thermogravimetric Analyses*

The samples were heated at a rate of 5°C/mn under an argon flow after isotherm treatment at 50°C in order to eliminate the adsorbed water.

(α) *V–Mo–O system.* The $H_x(V_xMo_{1-x})O_3 \cdot nH_2O$ phases show the same behavior whatever the x value. We present the TGA curve of the $H_{0.13}(V_{0.13}Mo_{0.87})O_3 \cdot nH_2O$ phase (Fig. 6a). After elimination of the adsorbed water, the structural water of the acidic product is lost (≅0.3 H_2O) from 50 to 220°C and then a slow deprotonation occurs up to around 350°C, with a loss of the water molecules formed by the combination of protons with the framework oxygen atoms. In order to determine if these phases are free of Na, a cooling treatment is performed from 400°C to room temperature. In contrast to the behavior of $Na_{0.13}V_{0.13}Mo_{0.87}O_3$ which rehydrates quickly upon cooling (12), no rapid rehydration is observed for the $H_{0.13}V_{0.13}Mo_{0.87}O_3$ phase and only a progressive weight gain evaluated at 0.8% is observed (Fig. 6b).

(β) *V–W–O system.* After the adsorbed water departure, the TGA curve (Fig. 7) of the $H_{0.27}(V_{0.27}W_{0.73})O_3 \cdot 1/3H_2O$ phase shows a first loss of all the structural water (0.33 H_2O) at 250°C and a slow second water loss (0.14 H_2O) occurring at around 480°C. This phenomenon corresponds to the deprotonation of the phase.

(*d*) *XRD Analyses*

The XRD patterns were collected at room temperature. The alignment of the D5000 Siemens diffractometer was checked with standard reference materials. The zero error was measured to be less than 0.01°(2θ). The powder diffraction pattern was scanned in steps of 0.02°(2θ), and a fixed-time counting (45 sec) was used. A careful evaluation of peak positions has been carried out with a fitting program available in the PC software DIFFRAC-AT and least square refinements were made from observed data with the computer programs DICVOL91 (16) and NBS*AIDS83 (17).

(α) *V–Mo–O system.* Whatever the x value, XRD patterns of the pure and crystallized phases show similar peak positions. We give the data for the $H_{0.13}V_{0.13}Mo_{0.87}O_3 \cdot 0.3H_2O$ compound.

The XRD pattern of the $H_{0.13}V_{0.13}Mo_{0.87}O_3 \cdot 0.3H_2O$ phase (Table 2) is very similar to those described (i) by Olenkova *et al.* (11) for the h-MoO_3 type with a hexagonal double layer structure and (ii) by Davies (13) for mixed vanadium molybdenum oxides. As the cell parameters

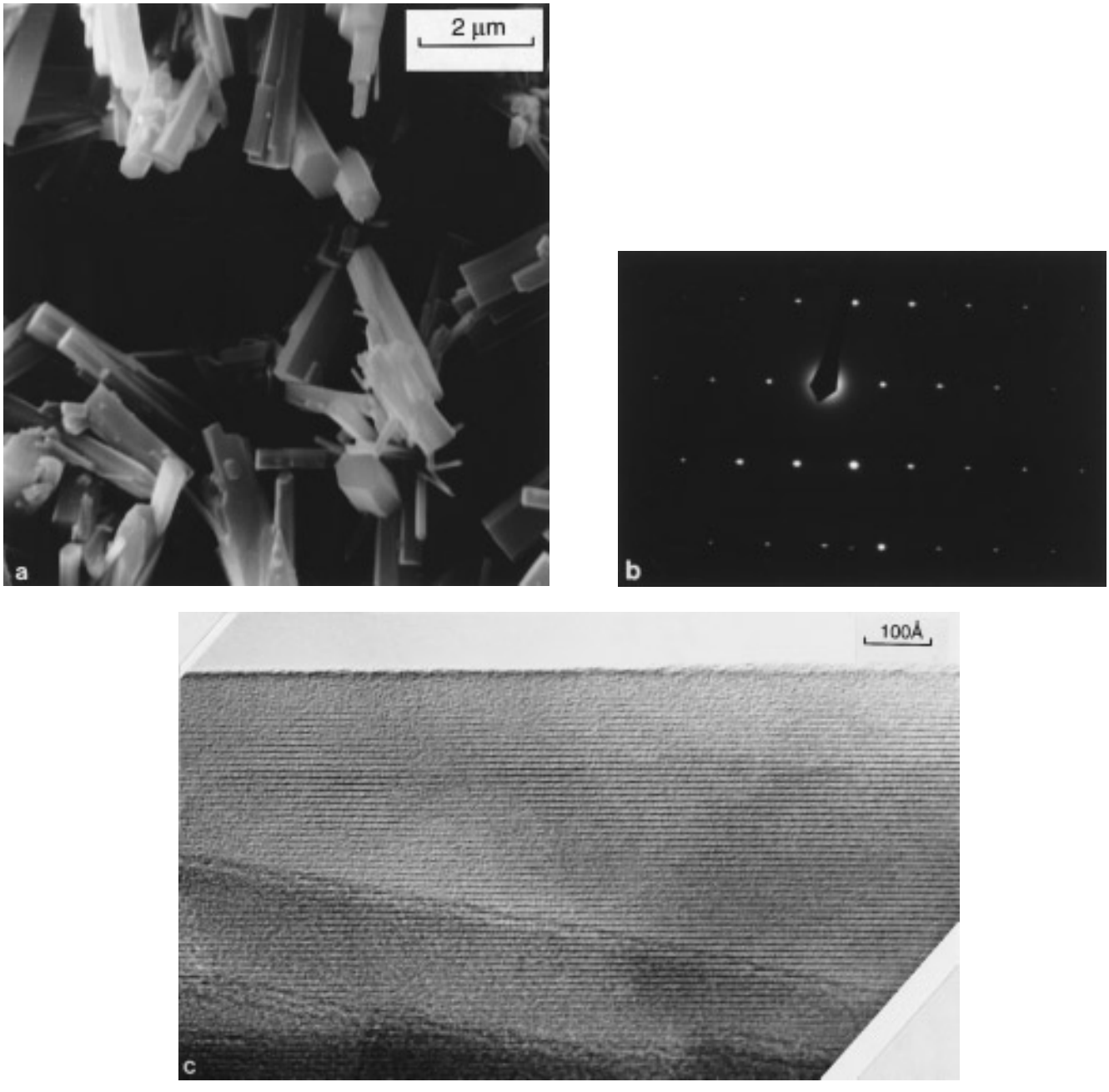

FIG. 8. (a) SEM micrograph of $H_{0.13}V_{0.13}Mo_{0.87}O_3 \cdot 0.3H_2O$ particles. (b) Microdiffraction pattern obtained on $H_{0.13}V_{0.13}Mo_{0.87}O_3 \cdot 0.3H_2O$ particles. (c) HREM observation of $H_{0.13}V_{0.13}Mo_{0.87}O_3 \cdot 0.3H_2O$ particles.

were approximately known (11, 13), a least square refinement from observed data was carried out. This refinement led to the figures of merit (18, 19) $M_{18} = 224.7$ and $F_{18} = 200.4$ (0.004, 22) for cell parameters $a = 10.6129(5)$ Å, $c = 3.7045(3)$ Å, and space group $P6_3$. These very high figures of merit values are an indication of the good assessment of the unit cell. These XRD data are listed in Table 2.

(β) *V–W–O system.* The XRD pattern of the $H_{0.27}V_{0.27}W_{0.73}O_3 \cdot 1/3H_2O$ phase (Table 3) is similar to that of the $WO_3 \cdot 1/3H_2O$ orthorhombic phase (20). The least square refinement from observed data leads to the figures of merit $M_{20} = 45.6$ and $F_{24} = 50.5$ (0.016, 30) for cell parameters $a = 7.276(1)$ Å, $b = 12.575(2)$ Å, $c = 7.726(1)$ Å, and space group *Fmm*2. These XRD data are listed in Table 3.

The small variation of cell volume (707.17 Å^3 for the V–W–O phase and 712.84 Å^3 for $WO_3 \cdot 1/3H_2O$) can be explained by the small difference between the

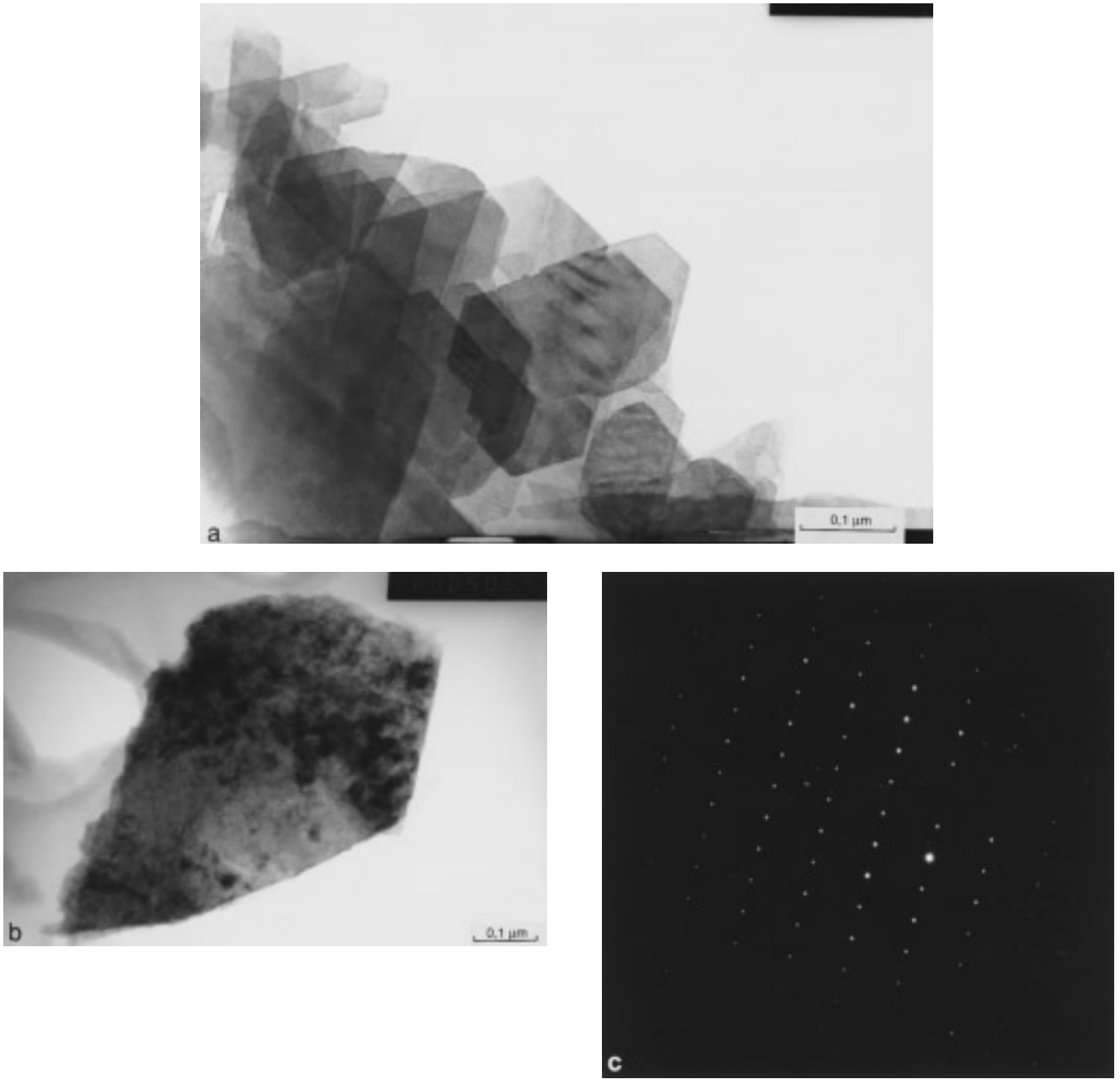

FIG. 9. TEM micrograph of $H_{0.27}V_{0.27}W_{0.73}O_3 \cdot 1/3H_2O$ particles obtained after (a) 1 week reaction and (b) 2 hr reaction. (c) Microdiffraction pattern obtained on $H_{0.27}V_{0.27}W_{0.73}O_3 \cdot 1/3H_2O$ particles. (d) HREM observation of $H_{0.27}V_{0.27}W_{0.73}O_3 \cdot 1/3H_2O$ particles.

ionic radii of V^{5+} and W^{6+} in octahedral coordination (21).

(*e*) *Electron Microscopy Studies*

(α) *V–Mo–O system.* The particles of the phases look like fine needles having 10-μm length and 1-μm width with hexagonal sections (Fig. 8a). These particles were beam sensitive as deduced by amorphization after a long time exposure under the electron beam. Based on the lattice parameters deduced from the least square refinement, it is possible to index the electron diffraction patterns (Fig. 8b). These particles lie mainly on the (100) or the (210) planes. The *c* axis of the hexagonal phase corresponds to the longer direction of the needles. The tunnels, parallel to the *c* axis, are then perpendicular to the direction of observation. HREM images of these particles (Fig. 8c) show large tunnels in the longitudinal section (the black

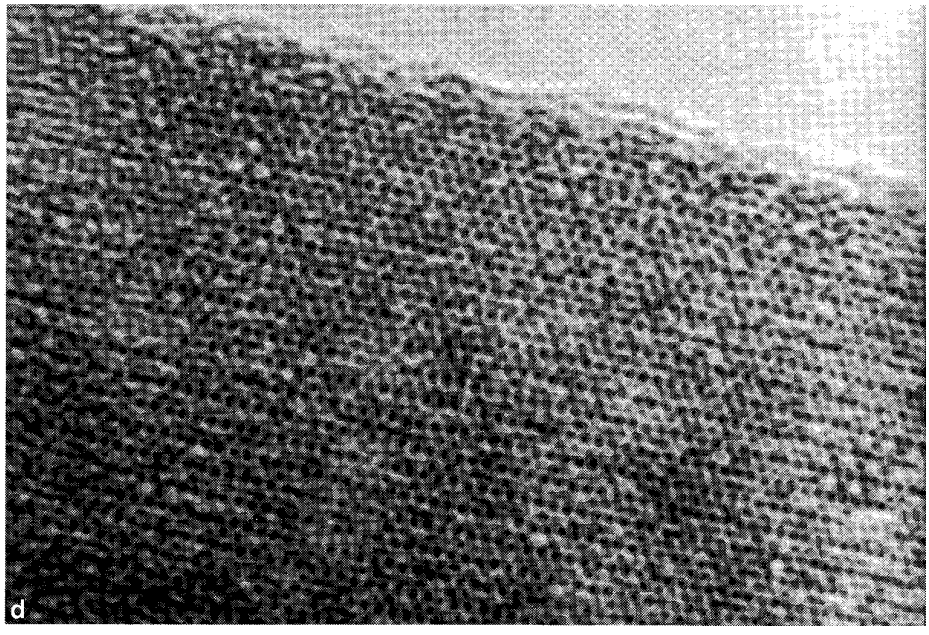

FIG. 9—*Continued*

slabs) and the white slabs represent the chains of octahedra. The measured distance between two reticular slabs, about 9.18 Å, is in good agreement with the d_{100} spacing value (9.20 Å).

(β) *V–W–O system.* The particles obtained after 1 week of reaction look like thin hexagonal platelets measuring 0.1 μm in diameter (Fig. 9a). If we observe these particles at the beginning of the reaction, they look like arrow heads (Fig. 9b). The growth of these particles is not complete as suggested by the arrow heads which are in fact one of the six vertices of the hexagonal platelets. These platelets lie on the (001) plane (Fig. 9c) and the *c* axis of the orthorhombic phase is parallel to the direction of observation. Due to the specific orientation, it will be easier to study this phase by HREM than the phases obtained in the V–Mo–O system. Nevertheless, this hydrated phase dehydrates under the combined effects of vacuum and electron beam. Then, it is very difficult to obtain monophasic electron diffraction pattern (Fig. 9c) and high resolution images of the hydrate (Fig. 9d). A complete HREM study of this phase is in progress.

V. CONCLUSION

By dissolution of metallic Mo or W and V_2O_5 in hydrogen peroxide, we obtained the hydrated mixed oxides $H_x(V_xMo_{1-x})O_3 \cdot 0.3H_2O$ ($0.06 \leq x \leq 0.18$) and $H_{0.27}V_{0.27}W_{0.73}O_3 \cdot 1/3H_2O$, respectively. This technique allowed us to cast off the presence of alkali in solution and then, later, in the cavities. Moreover, in comparison with Hu and Davies' work (13), we extended the existence domain of the hexagonal hydrated mixed vanadium molybdenum oxide.

REFERENCES

1. F. Harb, B. Gérand, G. Nowogrocki, and M. Figlarz, *Solid State Ionics* **32–33,** 84 (1989).
2. M. Figlarz, B. Dumont, B. Gérand, and B. Beaudoin, *J. Microsc. Spectrosc. Electron.* **7,** 371 (1982).
3. F. Harb, Thèse, Université de Picardie, Amiens, 1987.
4. F. Harb, B. Gérand, and M. Figlarz, *C.R. Acad. Sci. Paris Sér. II* **303(9),** 789 (1986).
5. C. Genin, Thèse, Université de Picardie, Amiens, 1992.
6. T. P. Feist and P. K. Davies, *Chem. Mater.* **3,** 1011 (1991).
7. N. Sotani, *Bull. Chem. Soc. Jpn.* **48(6),** 1820 (1975).
8. B. Krebs and I. Paulat-Böschen, *Acta Crystallogr. Sect. B* **32,** 1697 (1975).
9. E. M. MC Carron III, D. M. Thomas, and J. C. Calabrese, *Inorg. Chem.* **26,** 371 (1987).
10. B. Darriet and J. Galy, *J. Solid State Chem.* **8,** 189 (1973).
11. I. P. Olenkova, L. M. Plyasova, and S. D. Kirik, *React. Kinet. Catal. Lett.* **16,** 81 (1981).
12. P. K. Davies and C. M. Kagan, *Solid State Ionics* **53–56,** 546 (1992).
13. Y. Hu and P. K. Davies, *J. Solid State Chem.* **105,** 489 (1993).
14. J. Gopalakrishnan, G. N. Subbanna, and N. S. P. Bhuvanesh, *Chem. Mater.* **6,** 373 (1994).
15. I. Tsuyumoto, A. Kishimoto, and T. Kudo, *Solid State Ionics* **59,** 211 (1993).
16. A. Boultif and D. Louër, *J. Appl. Crystallogr.* **5,** 24 (1991).
17. A. D. Mighell, C. R. Hubbard, and J. K. Stalick, "NBS*AIDS80: a FORTRAN Program for Crystallographic Data Evaluation." Technical Note 1141. Natl. Bur. Standards, Washington, DC, 1981. [NBS*AIDS83 is an expanded version of NBS*AIDS80].
18. P. M. Wolff, *J. Appl. Crystallogr.* **1,** 108 (1968).
19. G. S. Smith and R. L. Snyder, *J. Appl. Crystallogr.* **12,** 60 (1979).
20. L. Seguin, Thèse, Université de Picardie, Amiens, 1994.
21. R. D. Shannon, *Acta Crystallogr. Sect. A* **32,** 751 (1976).